Hindawi
Advances in Civil Engineering
Volume 2021, Article ID 6675222, 10 pages
https://doi.org/10.1155/2021/6675222

Research Article

Research on Coal Mechanical Properties Based on True Triaxial Loading and Unloading Experiment

Yanyan Peng[1,2] **Haoxiang Deng**,[1,2] **Minghong Xing**,[1,2] **Pengfei Guo**[1,2] **and Chun Zhu**[1,2,3]

[1]*School of Civil Engineering, Shaoxing University, Shaoxing 312000, China*
[2]*Key Laboratory of Rock Mechanics and Geohazards of Zhejiang Province, Shaoxing 312000, China*
[3]*School of Earth Sciences and Engineering, Hohai University, Nanjing 210098, China*

Correspondence should be addressed to Chun Zhu; zhuchuncumtb@163.com

Received 4 December 2020; Revised 19 February 2021; Accepted 5 March 2021; Published 16 March 2021

Academic Editor: Hualei Zhang

To study the safety issues caused by coal mine excavation, self-developed simulation of earth interior atmosphere and sound test system was used to perform true triaxial loading and unloading tests of coal. An acoustic emission detection system was used to record the damage evolution trend of coal under different intermediate principal stress states. The experimental results show that in the true triaxial unloading test, as the intermediate principal stress increases, the failure state of coal changes from shear failure to partial shear tension failure, finally leading to overall yield failure. In the stress-strain curves, with the increase in intermediate principal stress, the strain in the direction of intermediate principal stress gradually changes from compression to expansion, and typical expansion occurs. The Mogi–Coulomb strength criterion better reflects the strength failure characteristics of coal during unloading. The stress-acoustic emission diagrams show that the increase in intermediate principal stress causes the internal cracks of the coal to grow unsteadily and exponentially, and the increase in intermediate principal stress makes the coal lose its ability to continue to bear the load. Studying the influence of the intermediate principal stress on the mechanical properties of coal has practical significance for coal mine safety production.

1. Introduction

In coal mining engineering, the deep underground engineering rock mass is in a three-way stress state [1–4]. Excavation of slopes, tunnels, or mines causes strong expansion of rock mass in the area adjacent to excavation surface, accompanied by complex mechanical failures such as tension and shear. Therefore, to study the mechanical properties of deep underground engineering rock mass, it is not enough to rely on uniaxial compression, tensile tests, or conventional triaxial compression tests only. True triaxial tests are needed to simulate the real force of rock mass.

In recent years, a large number of indoor true triaxial test studies have been conducted [5–12]. For example, He et al. [13, 14] carried out true triaxial unloading tests on limestone, sandstone, and granite samples in deep high in situ stress areas and obtained their rockburst induction mechanism and failure characteristics. Lü et al. [15] conducted a true triaxial unloading test on granite and derived a mechanical constitutive equation in the strain space considering the degradation effect of rock deformation parameters. Wang et al. [16] used a true triaxial testing machine to perform a series of loading and unloading tests on rock samples under compression and shear and obtained the variation trends of elastic shear modulus at different unloading stages. He et al. [17, 18] conducted a series of true triaxial simulation experiments and developed a new experimental method to simulate rockburst. Zhang et al. [19] conducted true triaxial loading and unloading confining pressure tests on marble and found that the energy dissipation of marble is related to the rate of unloading confining pressure. Li et al. [20] performed a true triaxial loading test of sandstone combined with CT scanning technology and systematically studied the characteristics of sandstone

strength and deformation under different intermediate principal stress conditions. Xue and Liu [21] used a true triaxial testing machine to simulate the underground stress conditions of a mine and combined with acoustic emission equipment made an early warning of coal mass destruction. Xi et al. [22] used a true triaxial THMC coupling test machine to study the thermal deformation and expansion coefficient of granite. Xie et al. [23–25] used true triaxial tests to study the mechanical behavior of rocks during deep mining.

At present, there are relatively few true triaxial test studies on the influence of intermediate principal stress on coal mechanical properties. Therefore, in this study, coal was taken as the research object; through true triaxial loading and unloading tests, the transient unloading failure of coal under the original rock stress state is simulated [26, 27], and acoustic emission detection technology was used to evaluate the effect of intermediate principal stress on coal strength and failure. The true triaxial test is used to study the influence of the intermediate principal stress on the mechanical properties of coal, which is of great significance to the safe mining of coal mines.

2. Experimental

2.1. Testing Machine. The true triaxial loading and unloading test device is composed of a test system simulation of earth interior atmosphere and sound. The equipment uses six rigid independent loading modules in three directions to simulate the three-dimensional stress state of deep underground engineering. The equipment can be loaded in three directions and six sides to a certain stress state and then can be quickly unloaded on one side. The indenter quickly unloads within 20 ms, and the free fall time is 176 ms. The specimen can be exposed on one side in 196 ms. The maximum tensile and compression test force of the three-way six-sided loading actuator is 1000 kN, and the maximum range is 300 mm. The equipment is shown in Figure 1(a).

The acoustic emission system uses PCI equipment produced by American Physical Acoustics. The equipment is composed of six preprobes, six signal amplifiers, AE win system host, and corresponding pipelines. It can collect information such as impact count, amplitude, energy, and spatial positioning of coal during destruction. A schematic of acoustic emission detection system is shown in Figure 1(b).

2.2. Sample Preparation. In this study, coal was selected as the research object. Coal was taken from the mining face in Shenshan Village, Tongchuan Town, Ordos City, Inner Mongolia Autonomous Region. To maintain the original stress state of sample, a large coal mass was selected from the mining face for processing. The coal sample was ground, so that the horizontal and vertical nonparallelism is less than 0.02 mm to form a coal sample of 100 mm × 100 mm × 100 mm, and wrapped with a plastic wrap. The average density of coal is 1578 kg/m^3, Poisson's ratio $\mu = 0.31$, elastic modulus $E = 1.75$ GPa, average peak compressive strength $\sigma_c = 14.6$ MPa, cohesion $c = 0.41$, and internal friction angle $\varphi = 41.3$. A photograph of the rock sample is shown in Figure 2.

2.3. Experimental Scheme. To study the mechanical properties of coal under the effect of different intermediate principal stresses, the tests are divided into groups 1 to 4, corresponding to the intermediate principal stresses of 3, 6, 9, and 12 MPa. Two coal samples were taken from adjacent sampling positions as one group: one for true triaxial loading test and the other for true triaxial unloading test.

In this test, the stress control method was used for loading, and each test system can automatically collect relevant data and draw the correlation curve of stress, impact count, energy count, and time. The test method is described below, and the relevant test data are shown in Table 1. Sample 1-L represents the first sample of true triaxial loading experiment, and sample 1-U represents the first sample of true triaxial unloading experiment.

(1) True triaxial loading test: load coal to the hydrostatic pressure state ($\sigma_1 = \sigma_2 = \sigma_3$) at a rate of 0.2 MPa/s; keep σ_3 unchanged; continue to load σ_1, σ_2 to the set value ($\sigma_1 = \sigma_2 > \sigma_3$) at a rate of 0.2 MPa/s; keep σ_2 unchanged; and continue to load σ_1 at a rate of 0.2 MPa/s until the coal is broken.

(2) True triaxial unloading test: the stress loading process is the same as above; when loading σ_1 at a rate of 0.2 MPa/s, load σ_1 to 90% of the axial stress σ_1 obtained when the coal is destroyed in the true triaxial loading test and keep σ_1, σ_2 constant. Then, unload σ_3 at a rate of 0.5 MPa/s (transient unloading) and observe the damage of coal.

During the test, the loading system and acoustic emission system should be kept synchronized in time. The acoustic emission system monitors the entire process of test coal failure and collects and analyzes relevant data.

3. Analysis of Experimental Results of Coal Samples

3.1. Failure Analysis. Figure 3 shows the characteristics of coal failure sections in true triaxial unloading tests under different intermediate principal stresses. Along the unloading direction, the coal has lateral expansion, and tensile fragments appear near the unloading surface.

When the intermediate principal stress is 3 MPa, small cracks appear on the unloading surface, and the crack direction and unloading direction have a certain angle between them. They expand along the unloading surface, showing obvious signs of shear friction. The failure mode of coal appears as shear failure, as shown in Figure 3(a).

When the intermediate principal stress is 6 MPa, vertical rough tension cracks appear near the unloading surface, locally accompanied by shear cracks. The failure mode of coal appears as a partial shear tension failure, as shown in Figure 3(b).

When the intermediate principal stresses are 9 MPa and 12 MPa, not only partial shear tension failure cracks appear

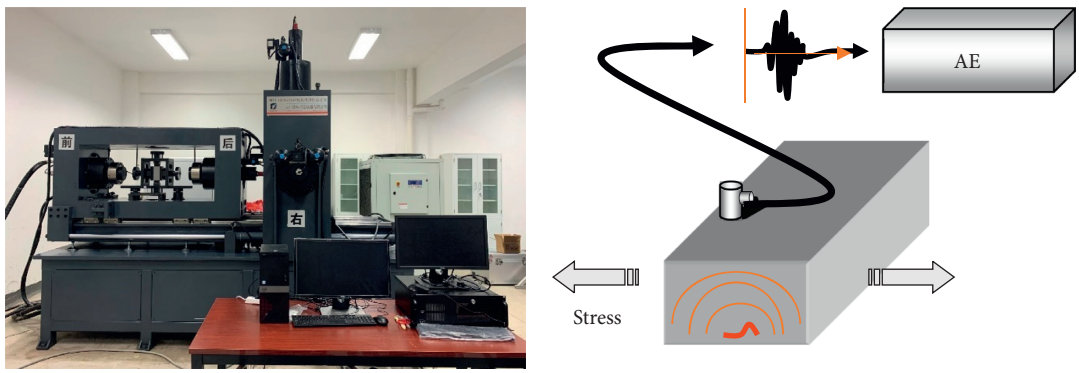

(a) (b)

Figure 1: Test system simulation of earth interior atmosphere and sound. (a) Earth interior atmosphere and sound experiment host. (b) Schematic of acoustic emission detection system.

Figure 2: Coal samples.

Table 1: True triaxial loading and unloading test data.

	True triaxial loading test				True triaxial unloading test			
Specimen number	1-L	2-L	3-L	4-L	1-U	2-U	3-U	4-U
σ_1 (MPa)	44.2	59.5	50.9	60.1	39.8	53.5	45.8	54.1
σ_2 (MPa)	3	6	9	12	3	6	9	12
σ_3 (MPa)	2				2			
Loading rate (MPa·s^{-1})	0.2				0.2			
Unloading rate (MPa·s^{-1})	0.5				0.5			

in the coal near the unloading surface but also shear cracks penetrate the entire coal, resulting in yield failure, as shown in Figures 3(c) and 3(d).

The failure mode of entire coal shows that with the increase in intermediate principal stress, the fracture surface of coal specimens and the number of crushed coal pieces also gradually increase, and the overall coal gradually develops a higher degree of fracture. Compared with Figure 3(a), the axial stress and lateral stress in Figure 3(d) have a greater impact on the coal sample. The internal microcracks are affected by transverse expansion tensile stress. When the stress at the ends of microcracks exceeds the shear strength of material at any time, the tension cracks on the outer surface of coal have a higher degree of development, and they have a clear positive correlation with the intermediate principal stress. At the same time, the number of cracks on the outer surface of coal specimens gradually increased. The cracks along the unloading direction divide the coal into several independent blocks, with the main fracture surface consistent with the direction of intermediate principal stress, indicating that the intermediate principal stress increased. In this case, the damage of specimen is mainly tensile and yield failure.

3.2. Deformation Analysis. Figure 4 shows the stress-strain relationship curves of true triaxial unloading tests under different intermediate principal stresses. ε_1 is the axial strain; ε_2 is the strain in the intermediate principal stress direction; ε_3 is the strain in the minimum principal stress direction; and ε_v is the volumetric strain, as shown in Figure 4.

(1) When the values of intermediate principal stress σ_2, σ_3 are relatively close, the stress-strain curve in the loading stage is similar to the conventional triaxial loading test. Coal underwent a development process from the compaction of original fissures to the initiation of new fissures and then to the interpenetration of fissures. Coal accumulates a certain amount of elastic potential energy during the loading stage. The curve tends to be horizontal after unloading, and brittle failures such as tension and shear occur [28–30].

(2) With the increase in intermediate principal stress σ_2, the deformation range of curve ε_3 in the loading stage also continues to widen. This is because the deformation in the ε_2 direction is constrained, and the Poisson effect causes lateral expansion in the ε_3 direction, resulting in increased deformation.

(3) With the increase in intermediate principal stress σ_2, curve ε_2 has an obvious inflection point, indicating that strain b is first compressed and then expanded. Curve ε_v has a significant slowdown or even rotation, indicating that the volumetric strain tends to expand.

3.3. Strength Analysis. Based on the Mises criterion theory, Mogi [31] found that intermediate principal stress has a

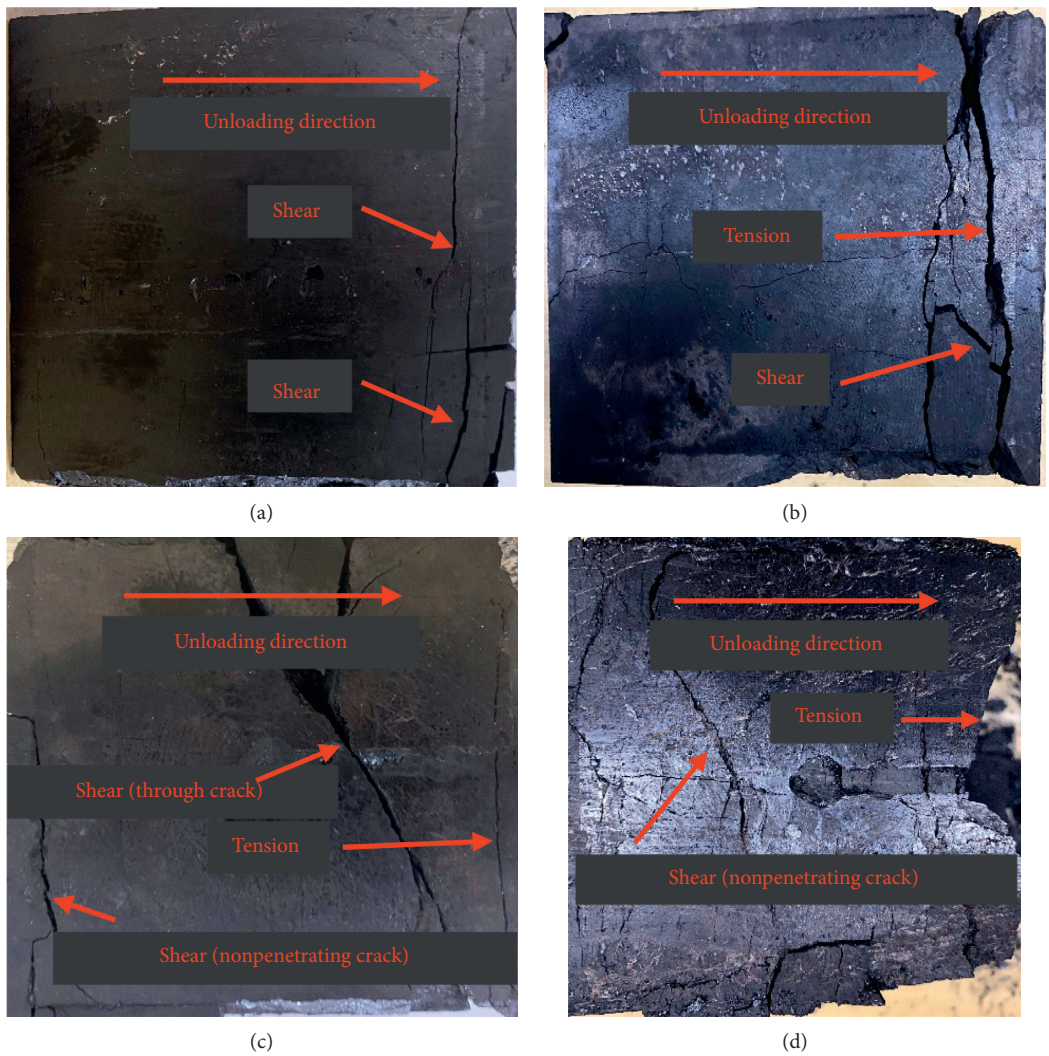

Figure 3: Failure section of coal in true triaxial unloading test. (a) Intermediate principal stress is 3 MPa. (b) Intermediate principal stress is 6 MPa. (c) Intermediate principal stress is 9 MPa. (d) Intermediate principal stress is 12 MPa.

significant effect on the strength of rock through true triaxial loading and unloading tests of various rocks. Therefore, an octahedral strength criterion considering the intermediate principal stress is proposed, the essence of which is still the shear failure criterion. The strength relationship between octahedral shear stress τ_{oct} and effective intermediate principal stress $\sigma_{m,2}$ at the time of failure can be expressed using equations (1) and (2):

$$\tau_{oct} = \frac{1}{3}\sqrt{(\sigma_1 - \sigma_3)^2 + (\sigma_1 - \sigma_2)^2 + (\sigma_2 - \sigma_3)^2}, \quad (1)$$

$$\sigma_{m,2} = \frac{\sigma_1 + \sigma_3}{2}. \quad (2)$$

Al-Ajmi and Zimmerman [32, 33] compiled a large number of true triaxial test data and found that after combining the Mogi empirical strength criterion with the Coulomb strength criterion, the $f(\sigma_{m,2})$ line-shape fit is ideal, namely, the Mogi–Coulomb strength criterion, which can be expressed using equations (3)–(6):

$$\tau_{oct} = \alpha + \beta\sigma_{m,2}, \quad (3)$$

$$\alpha = \frac{2\sqrt{3}}{3}c \cdot \cos\varphi, \quad (4)$$

$$\beta = \frac{2\sqrt{3}}{3}\sin\varphi, \quad (5)$$

$$\overline{\tau} = \frac{\sum ABS\left(\tau_{oct} - \tau_{oct}^{T}\right)}{N}, \quad (6)$$

where c is the cohesive force; φ is the angle of internal friction; α is the intercept between Mogi–Coulomb strength criterion fitting through a straight line and the τ_{oct}-axis; β is

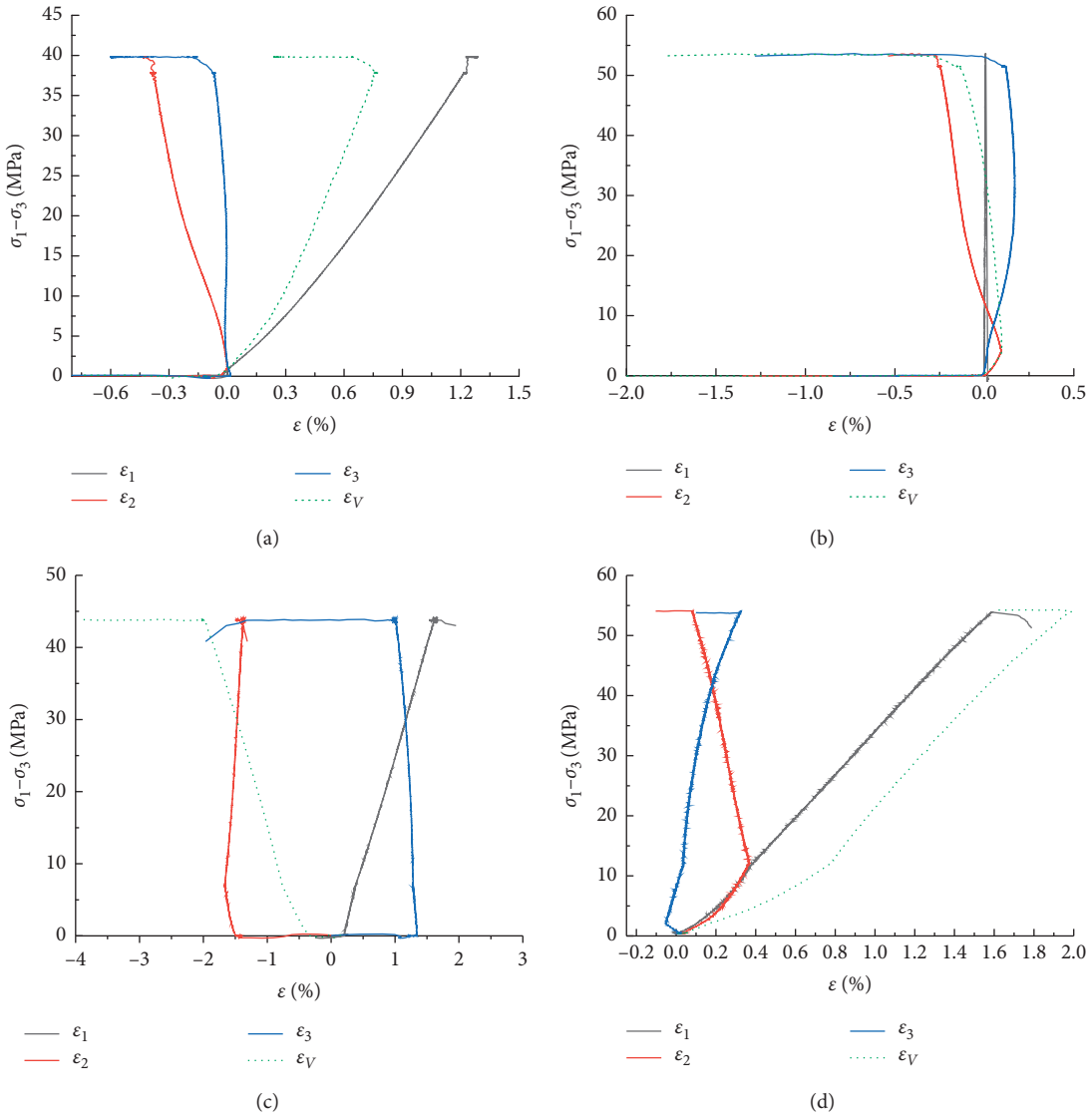

Figure 4: True triaxial unloading test stress-strain curve. (a) Intermediate principal stress is 3 MPa. (b) Intermediate principal stress is 6 MPa. (c) Intermediate principal stress is 9 MPa. (d) Intermediate principal stress is 12 MPa.

the slope of fitting straight line; $\overline{\tau}$ is the average deviation of octahedral shear stress intensity; τ_{oct} and τ_{oct}^{T} are the calculated and tested values; and N is the number of test groups.

To better reflect the strength failure characteristics of coal during unloading under high in situ stress conditions, a scatter plot was drawn using the transient unloading stress data of true triaxial unloading test, and the relationship curve between τ_{oct} and $\sigma_{m,2}$ was obtained by quadratic polynomial linear fitting, as shown in Figure 5.

According to the fitted quadratic polynomial curve, $\alpha = 0.4013$, $\beta = 0.7870$, $R^2 = 0.9688$, calculated cohesion $c = 0.47$, internal friction angle $\varphi = 42.9^{\circ}$, and the average deviation of the octahedral shear stress intensity $\overline{\tau} = 0.11$.

The calculated values of c and φ are relatively close to the test values measured by conventional triaxial loading test. Therefore, the Mogi–Coulomb strength criterion can better describe the strength failure characteristics of coal during unloading.

4. Analysis of Characteristics of Acoustic Emission Damage Evolution

Figure 6 shows the results of true triaxial unloading test (stress difference-acoustic emission) under different intermediate principal stresses.

Figure 6 shows that the characteristics of unloading acoustic emission under the condition of intermediate principal stress of coal have the following trends (because the failure of 9 MPa and 12 MPa of intermediate principal stress is similar, only 9 MPa is listed for explanation):

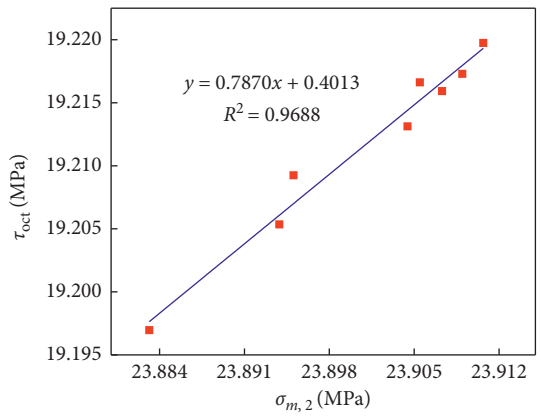

Figure 5: τ_{oct}-$\sigma_{m,2}$ relationship of true triaxial unloading test.

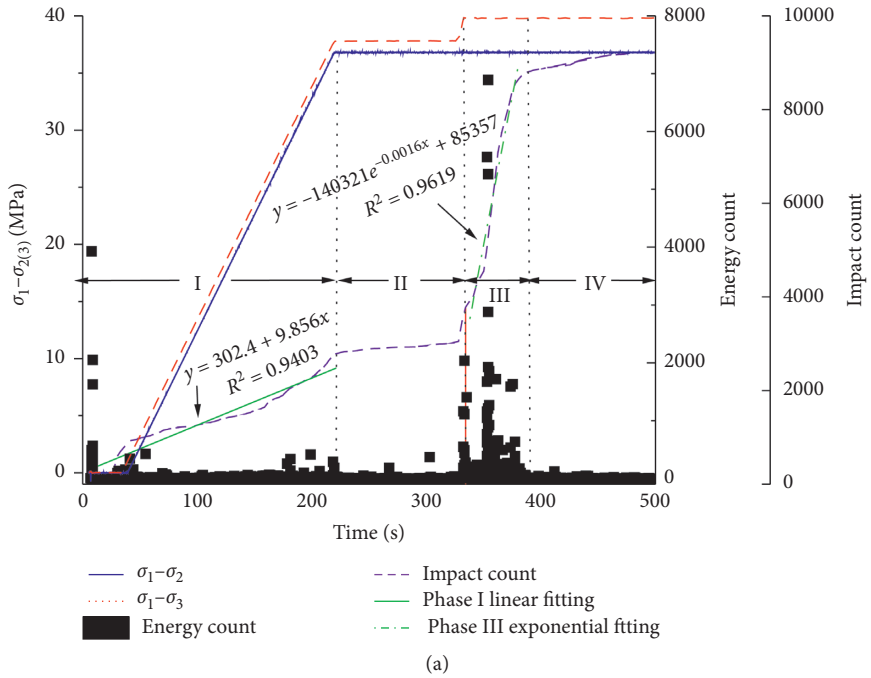

(a)

Figure 6: Continued.

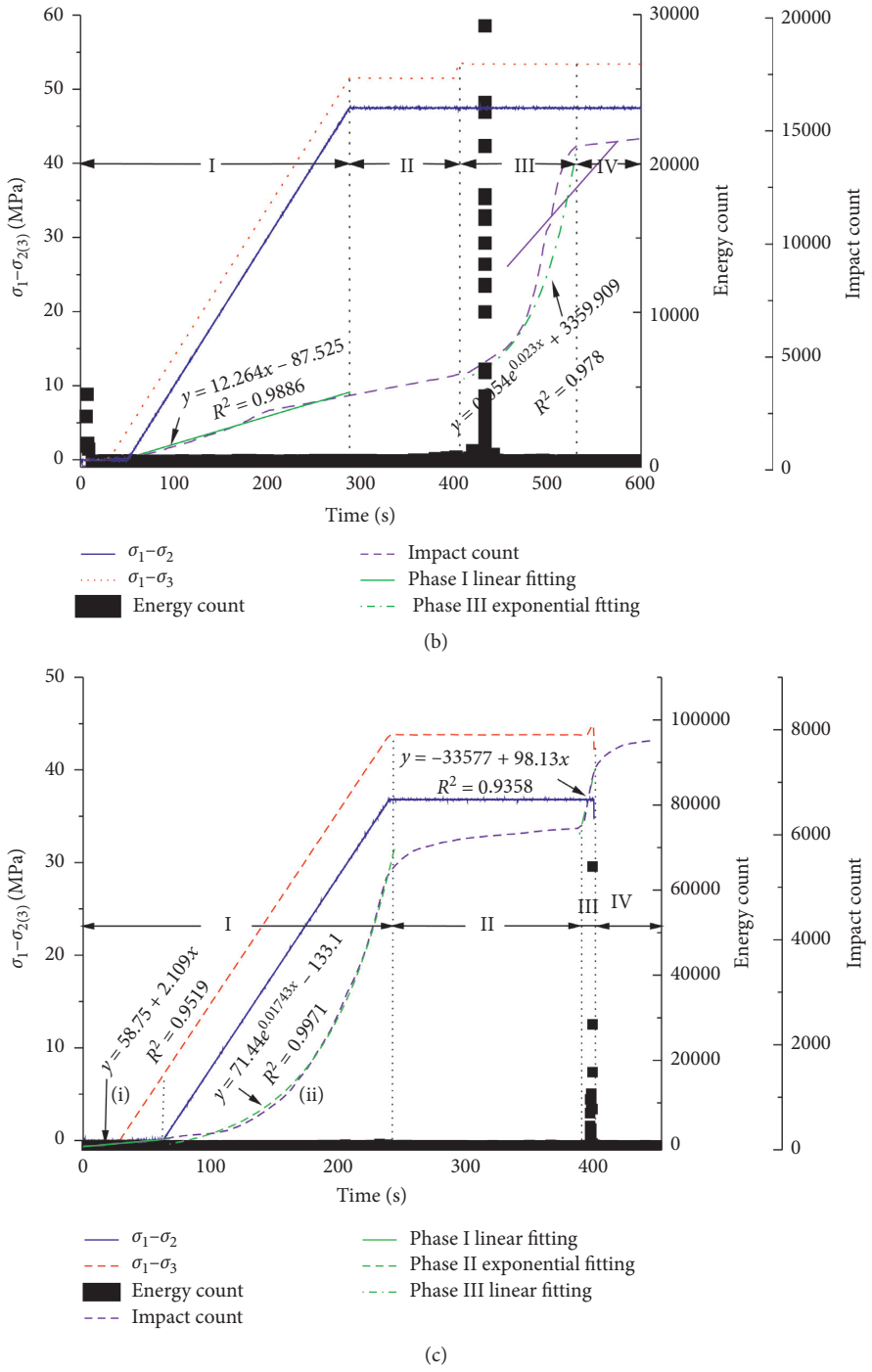

Figure 6: True triaxial unloading test of stress difference-AE curve. (a) Intermediate principal stress is 3 MPa. (b) Intermediate principal stress is 6 MPa. (c) Intermediate principal stress is 9 MPa.

(1) Loading (stage I): within a few seconds before the start of this stage, the acoustic emission energy count increases, and the stress difference is 0. This is because coal is deposited in a certain amount of original fissures in their natural state. As the test progresses, the fissures are continuously compacted [34]. Then, it enters the load. By fitting the impact count curve of stage I, the curve was found to be linearly distributed, and the energy count did not increase sharply, indicating that with the increase of load, the microcracks inside the coal begin to initiate and expand, and the elastic energy continues to accumulate. Thus, a steady growth trend was observed [35]. However, as a whole, the internal crack expansion is generated in a small area only, a linear elastic section [36], as shown in Figures 6(a) and 6(b) (stage I).

In addition, a longitudinal comparison showed that with the increase in intermediate principal stress, the

crack propagation in coal rapidly developed from a stable linear growth to an exponentially unsteady exponential growth, as shown in Figure 6(c) ((i) and (ii) of stage I).

(2) Confining pressure maintenance (stage II): to simulate the original stress state of coal so that it can more truly reflect the force of underground stress, this stage was set to maintain a stable time of 100 s to 150 s after maintaining linear loading. Loading was stopped at this stage. The stress difference and impact count curve are both horizontal, and the energy count has no major fluctuations.

(3) Unloading (stage III): in this stage, the minimum principal stress is unloaded. The two stress difference curves in the figure are separated, and the acoustic emission energy count sharply increases. After the impact count curve is fitted, it shows an exponential increase. This indicates that the internal pressure of coal after unloading the stored elastic energy is suddenly released, and the cracks formed inside penetrate each other, forming macroscopic cracks.

(4) Unloading completion (stage IV): at this stage, the coal has been destroyed, and the cracks have penetrated the entire coal. However, the impact count curve has not increased, and the energy count has not fluctuated, indicating that the rock mass still has a certain bearing capacity after failure [37–42], as shown in Figures 6(a) and 6(b) (stage IV). In addition, with the increase in intermediate principal stress, the coal has shown yield failure when entering stage IV, and the stress difference curve has a significant decline section, indicating that the intermediate principal stress makes the coal no longer able to continue to bear the load, as shown in Figure 6(c) (stage IV).

5. Conclusions

Through scientific experiments, the effect of intermediate principal stress on coal mechanical properties was evaluated. According to the effect of coal stability under different intermediate principal stresses, a prepeak unloading test was performed. Combining with the acoustic emission detection technology, obtain the coal failure law under the true triaxial unloading experiment. This research is of great significance to the study of the failure mechanism of coal mining:

(1) In the true triaxial unloading test, the deformation and failure characteristics of coal become severe with the increase in intermediate principal stress. The failure state develops from shear failure to partial shear tension failure, finally reaching yield failure. As the intermediate principal stress increases, the deformation in the direction of intermediate principal stress changes from compression to expansion, and capacity expansion occurs.

(2) The shear strength parameters calculated using the Mogi–Coulomb strength criterion are similar to those obtained experimentally. The Mogi–Coulomb strength criterion can better fit the true triaxial unloading strength of coal. This strength criterion accurately reflects the strength failure characteristics of coal during unloading when the intermediate principal stress changes.

(3) An increase in intermediate principal stress can cause unstable growth of cracks in the loading stage. During the unloading stage, the acoustic emission energy count increases significantly with the increase in intermediate principal stress, indicating that it has a certain effect on the accumulation of elastic energy in coal. In the unloading stage, when the intermediate principal stress is slight, the coal still has the bearing capacity, but with the increase in intermediate principal stress, the bearing capacity of coal decreases.

Data Availability

The data used to support the findings of this study are included within the article.

Conflicts of Interest

The authors declare that they have no conflicts of interest.

Acknowledgments

This research was supported by the National Natural Science Foundation of China (no. 41702381), Zhejiang Public Welfare Technology Research Program/Social Development (no. LGF20D020002), Key Laboratory of Rock Mechanics and Geohazards of Zhejiang Province (no. ZJRMG-2020-02), and Fundamental Research Funds for the Central Universities (no. B210201001).

References

[1] M. He and Q. Qian, *The Basis of Deep Rock Mechanics*, Science Press, Beijing, China, 2010.

[2] Y. Wang, C. H. Li, H. Liu, and J. Q. Han, "Fracture failure analysis of freeze-thawed granite containing natural fracture under uniaxial multi-level cyclic loads," *Theoretical and Applied Fracture Mechanics*, vol. 110, p. 102782, 2020.

[3] C. Zhu, M. C. He, Q. Yin, and X. H. Zhang, "Numerical simulation of rockfalls colliding with a gravel cushion with varying thicknesses and particle sizes," *Geomechanics and Geophysics for Geo-Energy and Geo-Resources*, vol. 7, p. 11, 2021.

[4] A. D. Alexeev, V. N. Revva, N. A. Alyshev, and D. M. Zhitlyonok, "True triaxial loading apparatus and its application to coal outburst prediction," *International Journal of Coal Geology*, vol. 58, no. 4, pp. 245–250, 2004.

[5] B. Li, R. Bao, Y. Wang, R. Liu, and C. Zhao, "Permeability evolution of two-dimensional fracture networks during shear under constant normal stiffness boundary conditions," *Rock Mechanics and Rock Engineering*, vol. 54, no. 3, pp. 1–20, 2021.

[6] Q. Wang, H. Gao, B. Jiang, S. Li, M. He, and Q. Qin, "In-situ test and bolt-grouting design evaluation method of underground engineering based on digital drilling," *International*

Journal of Rock Mechanics and Mining Sciences, vol. 138, p. 104575, 2021.

[7] Q. Wang, Q. Qin, B. Jiang et al., "Mechanized construction of fabricated arches for large-diameter tunnels," *Automation in Construction*, vol. 124, p. 10358, 2021.

[8] Q. Meng, H. Wang, M. Cai, W. Xu, X. Zhuang, and T. Rabczuk, "Three-dimensional mesoscale computational modeling of soil-rock mixtures with concave particles," *Engineering Geology*, vol. 277, p. 105802, 2020.

[9] C. Zhu, M. He, M. Karakus, X. Cui, and Z. Tao, "Investigating toppling failure mechanism of anti-dip layered slope due to excavation by physical modelling," *Rock Mechanics and Rock Engineering*, vol. 53, no. 11, pp. 5029–5050, 2020.

[10] Z. Tao, C. Zhu, M. He, and M. Karakus, "A physical modeling-based study on the control mechanisms of negative Poisson's ratio anchor cable on the stratified toppling deformation of anti-inclined slopes," *International Journal of Rock Mechanics and Mining Sciences*, vol. 138, p. 104632, 2021.

[11] Q.-X. Meng, W.-Y. Xu, H.-L. Wang, X.-Y. Zhuang, W.-C. Xie, and T. Rabczuk, "DigiSim-an open source software package for heterogeneous material modeling based on digital image processing," *Advances in Engineering Software*, vol. 148, p. 16, 2020.

[12] R. Jiang, F. Dai, Y. Liu, and A. Li, "Fast marching method for microseismic source location in cavern-containing rockmass: performance analysis and engineering application," *Engineering*, 2021.

[13] M. C. He, J. L. Miao, and J. L. Feng, "Rock burst process of limestone and its acoustic emission characteristics under true-triaxial unloading conditions," *International Journal of Rock Mechanics and Mining Sciences*, vol. 47, no. 2, pp. 286–298, 2010.

[14] H. Huang, T. Babadagli, X. Chen, H. Li, and Y. Zhang, "Performance comparison of novel chemical agents for mitigating water-blocking problem in tight gas sandstones," *SPE Reservoir Evaluation and Engineering*, vol. 23, no. 4, pp. 1150–1158, 2020.

[15] Y. H. Lü, Q. Liu, and H. Jiang, "Study of mechanical deformation characteristics of granite in unloading experiments of high stress," *Rock and Soil Mechanics*, vol. 31, no. 2, pp. 337–344, 2010.

[16] Y. Wang, S. Shao, Z. Wang, and A. Liu, "Experimental study on the unloading characteristics of coarse aggregate under true triaxial shear loading," *Chinese Journal of Rock Mechanics and Engineering*, vol. 39, no. 7, pp. 1503–1512, 2020.

[17] M. He, F. Zhao, W. Gong et al., "Investigation of unloading rockburst test based on acoustic emission," *Disaster Advances*, vol. 6, no. 6, pp. 322–330, 2013.

[18] M. C. He, F. Zhao, M. Cai, and S. Du, "A novel experimental technique to simulate pillar burst in laboratory," *Rock Mechanics and Rock Engineering*, vol. 48, no. 5, pp. 1833–1848, 2015.

[19] L. Zhang, S. Gao, Z. Wang et al., "Analysis of marble failure energy evolution under loading and unloading conditions," *Chinese Journal of Rock Mechanics and Engineering*, vol. 32, no. 8, pp. 1572–1578, 2013.

[20] W. Li, L. Wang, Y. Lu et al., "Experimental investigation on the strength, deformation and failure characteristics of sandstone under true triaxial compression," *Journal of Mining & Safety Engineering*, vol. 36, no. 1, pp. 191–197, 2019.

[21] S. Xue and J. Liu, "Long-range correlation characteristics of acoustic emission for coal samples subjected to true triaxial loading-unloading," *Journal of Safety Science and Technology*, vol. 16, no. 2, pp. 30–36, 2020.

[22] B. Xi, S. He, Y. Wu, Z. Cheng, and G. Xin, "Experimental study on evolution law of thermal deformation and thermal expansion coefficient of granite under in-situ stress state," *Rock and Soil Mechanics*, vol. 41, no. 2, pp. 1–11, 2020.

[23] H. Xie, H. Zhou, J. Liu et al., "Mining-induced mechanical behavior in coal seams under different mining layouts," *Journal of China Coal Society*, vol. 36, no. 7, pp. 1067–1074, 2011.

[24] L. Li, Z. Xu, H. Xie, Y. Ju, X. Ma, and Z. C. Han, "Failure experimental study on energy laws of rock under differential dynamic impact velocities," *Journal of China Coal Society*, vol. 36, no. 12, pp. 2007–2011, 2011.

[25] M. Gao, M. Wang, H. Xie et al., "In-situ disturbed mechanical behavior of deep coal rock," *Journal of China Coal Society*, vol. 45, no. 8, pp. 2691–2703, 2020.

[26] M. Cai, "Principles of rock support in burst-prone ground," *Tunnelling and Underground Space Technology*, vol. 36, pp. 46–56, 2013.

[27] D. Li, T. Xie, X. Li, and T. Wang, "On the Mogi-Coulomb strength criterion as applied to rock triaxial unloading test," *Science & Technology Review*, vol. 33, no. 19, pp. 84–90, 2015.

[28] P. Baud, T.-F. Wong, and W. Zhu, "Effects of porosity and crack density on the compressive strength of rocks," *International Journal of Rock Mechanics and Mining Sciences*, vol. 67, pp. 202–211, 2014.

[29] R. Yong, J. Ye, B. Li, and S.-G. Du, "Determining the maximum sampling interval in rock joint roughness measurements using Fourier series," *International Journal of Rock Mechanics and Mining Sciences*, vol. 101, pp. 78–88, 2018.

[30] B. Tarasov and Y. Potvin, "Universal criteria for rock brittleness estimation under triaxial compression," *International Journal of Rock Mechanics and Mining Sciences*, vol. 59, pp. 57–69, 2013.

[31] K. Mogi, *Experimental Rock Mechanics*, Taylor & Francis Group, London, UK, 2007.

[32] A. M. Al-Ajmi and R. W. Zimmerman, "Relation between the Mogi and the Coulomb failure criteria," *International Journal of Rock Mechanics and Mining Sciences*, vol. 42, no. 3, pp. 431–439, 2005.

[33] A. M. Al-Ajmi and R. W. Zimmerman, "Stability analysis of vertical boreholes using the Mogi-Coulomb failure criterion," *International Journal of Rock Mechanics and Mining Sciences*, vol. 43, no. 8, pp. 1200–1211, 2006.

[34] A. Li, R. Zhang, A. I. Ting et al., "Acoustic emission space-time evolution rules and failure precursors of granite under uniaxial compression," *Chinese Journal of Geotechnical Engineering*, vol. 38, no. 2, pp. 306–311, 2016.

[35] D.-S. Cheon, Y.-B. Jung, E.-S. Park, W.-K. Song, and H.-I. Jang, "Evaluation of damage level for rock slopes using acoustic emission technique with waveguides," *Engineering Geology*, vol. 121, no. 1-2, pp. 75–88, 2011.

[36] B. Liu, J. Huang, Z. Wang et al., "Study on damage evolution and acoustic emission character of coal-rock under uniaxial compression," *Chinese Journal of Rock Mechanics and Engineering*, vol. 28, no. 1, pp. 3234–3238, 2009.

[37] Y. C. Lü and H. Qin, "Investigation into mechanical responses and energy dissipation properties of coal containing methane to confinement unloading," *Journal of China Coal Society*, vol. 37, no. 9, pp. 1505–1510, 2012.

[38] L.-L. Yang, W.-Y. Xu, Q.-X. Meng, and R.-B. Wang, "Investigation on jointed rock strength based on fractal theory," *Journal of Central South University*, vol. 24, no. 7, pp. 1619–1626, 2017.

[39] Q. Meng, L. Yan, Y. Chen, and Q. Zhang, "Generation of numerical models of anisotropic columnar jointed rock mass using modified centroidal voronoi diagrams," *Symmetry*, vol. 10, no. 11, p. 618, 2018.

[40] Z. Tao, C. Zhu, X. Zheng et al., "Failure mechanisms of soft rock roadways in steeply inclined layered rock formations," *Geomatics, Natural Hazards and Risk*, vol. 9, no. 1, pp. 1186–1206, 2018.

[41] W. Wang, L.-Q. Li, W.-Y. Xu, Q.-X. Meng, and J. Lü, "Creep failure mode and criterion of Xiangjiaba sandstone," *Journal of Central South University*, vol. 19, no. 12, pp. 3572–3581, 2012.

[42] H. Huang, T. Babadagli, H. Z. Li, K. Develi, and D. S. Zhou, "A visual experimental study on proppants transport in rough vertical fractures," *International Journal of Rock Mechanics and Mining Sciences*, vol. 134, p. 104446, 2020.